nature communications

Article

https://doi.org/10.1038/s41467-026-72863-1

Structural insights into YheS-mediated release of SecM-arrested ribosome

Received: 10 September 2025

Accepted: 23 April 2026

Published online: 09 June 2026

Check for updates

Kaishi Iso[1,6], Toma Ikeda[2,6], Kohei Yamasaki[3,6], Yushin Ando[1], Fumiya K. Sano[1], Tadaomi Furuta[2], Hideki Taguchi[2,4] ✉, Osamu Nureki[1,4] ✉, Yuhei Chadani[5] ✉ & Yuzuru Itoh[1] ✉

ATP-binding cassette subfamily F (ABCF) proteins interact with the ribosome to resolve translation defects near the peptidyl transferase center (PTC). In *Escherichia coli*, four ABCF proteins (EttA, Uup, YbiT, and YheS) selectively promote translation of distinct problematic nascent peptide sequences, but their molecular mechanisms remain unclear. Here, we present a 2.8 Å cryo-EM structure of the ribosome in complex with an ATPase-deficient mutant of YheS and investigate how it releases ribosomes arrested by the SecM nascent chain. YheS binds to the ribosomal E-site via the L1 stalk, and its P-site tRNA-interaction motif (PtIM) extends toward the PTC, displacing the CCA end of the P-site tRNA. Notably, the cryo-EM density corresponding to the SecM nascent chain within the exit tunnel is largely lost upon YheS binding. These observations suggest that YheS relieves peptide sequence-dependent stalling by perturbing nascent chain-tunnel interactions through P-site tRNA relocation. Steered molecular dynamics simulations provide qualitative support for this model. Together, our findings provide mechanistic insight into a mode of arrest release distinct from the translocon-mediated release mechanism.

The immense diversity of amino acid sequences underpins the functional complexity of proteins. However, it has become evident that ribosomes have difficulties with polymerizing certain amino acid sequences, including stretches of proline, tryptophan, charged residues, or ribosome-arresting peptides, due to interactions within the peptide exit tunnel[1–15]. Genome-wide and structural studies suggest such problematic sequences are widespread and become more deleterious under stress or aging conditions[16–21].

Remarkably, cells have evolved to harness such difficult events for gene regulation. In *E. coli*, the SecM nascent-polypeptide chain arrests the ribosome through interactions within the exit tunnel, thereby promoting the expression of the downstream translocase SecA[11,22–27]. The stalled ribosome is subsequently released by an external pulling force generated by the Sec translocon, exemplifying a mechanical strategy for programmed translation arrest.

To minimize the risks posed by such problematic sequences, cells have also evolved specialized translation factors. One example is EF-P (or eIF5A in eukaryotes), which alleviates stalling at polyproline stretches by binding to the ribosomal E site[4,5,28]. In parallel, members of the ABCF (ATP-binding cassette subfamily F) family have emerged as additional modulators of translation difficulties[29,30]. Among them, antibiotic resistance (ARE)-ABCFs dislodge antibiotics from the exit tunnel by inserting a long interdomain linker (~110 aa) that relocates the P-site tRNA (P-tRNA)[31–35]. In contrast, non-ARE ABCFs, comprising EttA, Uup, YbiT, and YheS in *E. coli*, possess shorter interdomain linkers (~80 aa), termed the P-tRNA-interaction motif (PtIM). While EttA

[1]Department of Biological Sciences, Graduate School of Science, The University of Tokyo, Tokyo, Japan. [2]School of Life Science and Technology, Institute of Science Tokyo, Yokohama, Japan. [3]Graduate School of Environmental, Life, Natural Science and Technology, Okayama University, Okayama, Japan. [4]Cell Biology Center, Institute of Integrated Research, Institute of Science Tokyo, Yokohama, Japan. [5]Faculty of Environmental, Life, Natural Science and Technology, Okayama University, Okayama, Japan. [6]These authors contributed equally: Kaishi Iso, Toma Ikeda, Kohei Yamasaki. ✉e-mail: taguchi@bio.titech.ac.jp; nureki@bs.s.u-tokyo.ac.jp; ychadani@okayama-u.ac.jp; yuzuru.itoh@bs.s.u-tokyo.ac.jp

promotes elongation immediately after initiation[36–38], the functions of the other non-ARE ABCFs have remained unclear.

Recently, we and others have demonstrated that these four ABCFs manage the "hard-to-translate" amino acid sequences[39–42]. A key finding is that the four ABCFs exhibit "sequence specificity", targeting distinct challenging motifs. For example, YheS, but not the other ABCFs, specifically releases the SecM-arrested ribosome. Despite their predicted structural similarity, the molecular basis for the YheS-specific release of SecM-induced translation arrest has remained elusive.

In this study, we investigated the mechanism by which YheS alleviates SecM-induced ribosome stalling, using single-particle cryogenic-electron microscopy (cryo-EM), complemented by molecular dynamics (MD) simulations. We determined the structure of the SecM-arrested ribosome in complex with the ATPase-deficient YheS mutant (EQ_2) at 2.82 Å resolution. YheS occupies the ribosomal E site and its PtIM protrudes toward the peptidyl transferase center (PTC), forming extensive contacts with the 50S large subunit (LSU) and relocating the P-tRNA. This is accompanied by a ~ 2 Å retraction of the SecM nascent chain. Together, these structural findings, supported by MD simulations, suggest that YheS facilitates the release of the SecM-arrested ribosome through a mechanism distinct from the Sec translocon-mediated release mechanism.

Results

Overall structure of YheS bound to the SecM-arrested ribosome complex

ABCF proteins act on the ribosome to resolve translational defects, and subsequently hydrolyze ATP upon their dissociation[29,36]. To prevent dissociation from the ribosome, we used an ATPase-deficient mutant of YheS (E175Q/E456Q, referred to as EQ_2)[40]. The SecM-arrested ribosome was reconstituted using the *E. coli* cell-free PURE system[43], and then combined with the purified YheS-EQ_2 mutant. In this study, we employed the SecM Glu134–Leu169 segment, which induces translational arrest and is released by YheS in a manner equivalent to full-length SecM[40,44] (Supplementary Fig. 1). The resulting complex was directly applied to cryo-EM grids without further purification. Cryo-EM particles were classified based on the rotation state of the 30S small subunit (SSU) and the occupancy at the A, P, and E sites, using focused masks targeting these regions (Supplementary Fig. 2). We successfully obtained cryo-EM maps of SecM-arrested ribosomes containing A-site tRNA (A-tRNA) and P-tRNA, both with and without YheS, at overall resolutions of 2.82 and 2.89 Å, respectively (Supplementary Fig. 3 and Supplementary Table 1 and 2). In both reconstructions, the codon-anticodon densities are consistent with the expected SecM-arrested state, in which $tRNA^{Pro}$ and $tRNA^{Gly}$ occupy the A and P sites, respectively (Supplementary Fig. 4). The structure of the SecM-arrested ribosome without YheS closely resembles the previously reported structure (PDB ID: 8QOA)[27], with the exception that the observed SecM segment spans residues 136–165, four residues shorter than those resolved in the prior model (Supplementary Fig. 5a, b). The ribosome structure of this complex without YheS is generally the same as those of the elongating ribosomes [45,46].

YheS binds to the ribosomal E site and interacts with multiple components, including the 23S rRNA near the E site and the peptidyl transferase center (PTC), the L1-stalk, uS7 of the SSU head, and the P-tRNA (Fig. 1a, b). Within the exit tunnel, only the C-terminal three residues of the SecM nascent chain (Arg163-Ala164-Gly165) are resolved (Fig. 1c), whereas upstream segments are largely invisible, with only weak and uninterpretable residual densities remaining (Supplementary Fig. 5c). Structurally, YheS forms a pseudo-dimer composed of two nucleotide-binding domains (NBD1 and NBD2), each containing conserved ABC motifs, including the Walker A (P-loop), Walker B, H-switch, Q-loop, D-loop, A-loop, and signature motifs (Fig. 1d, e)[47]. NBD1 also contains an "Arm" subdomain (residues 90–121) that interacts with the L1-stalk. The two NBDs are connected by a long helix-turn-helix element, PtIM (residues 230–312), which protrudes toward the PTC and interacts with both the 23S rRNA and the acceptor arm of the P-tRNA. The C-terminal extension of YheS (residues 527–637) is not visible.

ATP interactions in YheS

Two ATP molecules (ATP1 and ATP2) are bound to the P-loops of NBD1 and NBD2, respectively (Fig. 1f, g, Supplementary Fig. 6). At the ATP1 site, the main-chain amide groups of Gly37, Gly39, Lys40, and Ser41, along with the side chains of Lys40 and Thr42, form hydrogen bonds with the phosphate groups of the ATP molecule (Fig. 1f). A Mg^{2+} ion is coordinated by the β and γ phosphates of ATP1, as well as by the side chains of Ser41 and Gln71, further stabilizing the nucleotide binding. Additionally, the side chain of Arg14 interacts with the ribose moiety of ATP1 via a hydrogen bond. ATP2 is coordinated similarly by the corresponding conserved residues. While both ATP sites share a conserved binding mode, there are notable differences: Arg11 forms a π-stacking interaction with the adenine of ATP1, whereas the corresponding interaction at the ATP2 site is mediated by Tyr322 (Fig. 1g). Furthermore, the side chains of Lys423 and Glu435 form hydrogen bonds with the ribose of ATP1, whereas no such interactions are observed at the ATP2 site.

Importantly, the ATP binding sites are located at the interface between NBD1 and NBD2 (Fig. 1d, f and g). The γ-phosphate of ATP1 forms additional hydrogen bonds with the side chain of Ser432 and the main-chain of Gly434 from NBD2; equivalent interactions are mirrored at the ATP2 site with the corresponding residues in NBD1. An additional hydrogen bond is formed between Asp149 of NBD1 and the ribose of ATP2. Because these interdomain interactions are mediated by the γ-phosphate, ATP hydrolysis is expected to disrupt the NBD1–NBD2 interface. This would induce a conformational change of YheS, likely leading to its dissociation from the ribosome.

Arm interactions with the L1-stalk of LSU

The Arm subdomain of YheS interacts with both the protein and RNA components of the ribosomal L1-stalk of LSU, specifically uL1 and helix 76 (H76) of the 23S rRNA (Fig. 2a and b, Supplementary Table 3). Residues His114, Asp118, and Asp121 form hydrogen bonds or salt bridges with uL1, while Asn105 and Trp123 of YheS form stacking interactions with the uL1 residues. In parallel, Ser127, His134, and Asn140 hydrogen bond with the nucleotides in H76. The L1-stalk is typically flexible and thus often poorly resolved in structural studies[27,46], as is the case in our SecM-arrested ribosome without YheS. In contrast, it is well defined in our cryo-EM map with YheS (Fig. 1a), likely due to the stabilization by these extensive YheS-ribosome interactions. In addition, YheS interacts with helix 68 (H68) of domain IV in the 23S rRNA, adjacent to the L1-stalk. Residues Asn25 and Thr228 in NBD1, along with Gln244 (near the base of PtIM), form hydrogen bonds with the H68 nucleotides (Fig. 2c).

Interactions with the SSU head and the LSU central protuberance

NBD1 of YheS interacts with the ribosomal protein uS7 in the head of the SSU (Fig. 2d and Supplementary Fig. 7a). Residues Asn310, Pro311, Asn334, Ser339, and Asp496 form hydrogen bonds or salt bridges with uS7. These interactions appear to induce a ~ 6 Å shift of the SSU head, resulting in expansion of the E site space compared to the SecM-arrested ribosome without YheS (Supplementary Fig. 7a). A cis-peptide bond between Asn310 and Pro311 likely contributes to the formation of this specific interface (Fig. 2d). YheS also interacts with the central protuberance (CP) of the LSU, displacing it by ~5 Å (Supplementary Fig. 7a). Although no obvious hydrogen bonds are observed, NBD2 of YheS and the ribosomal protein uL5 in the CP are located within the van der Waals interaction distance (Supplementary Fig. 7b). Since the

https://doi.org/10.1038/s41467-026-72863-1

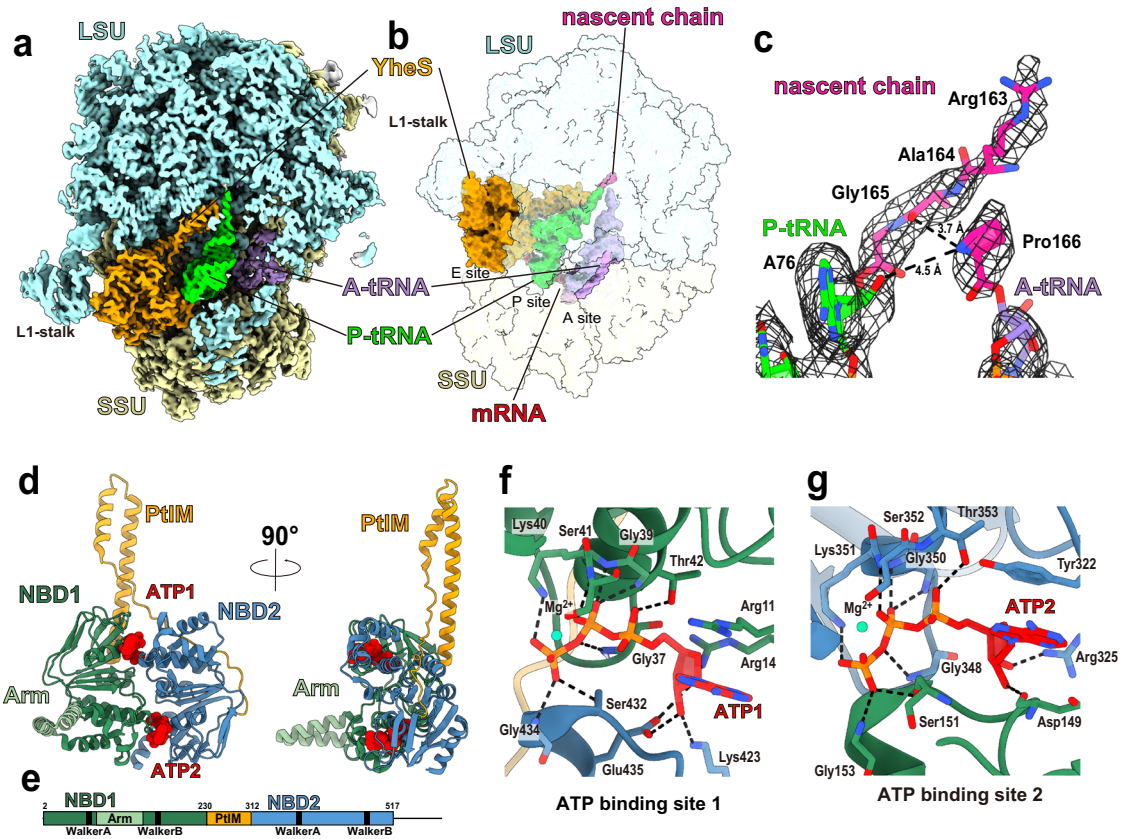

Fig. 1 | Cryo-EM structure of SecM-arrested ribosome in complex with YheS. **a** Overall cryo-EM map of the 70S ribosome with a cutaway view highlighting bound YheS. A- and P-tRNAs are present, and YheS is in the E site. The map without sharpening is used. **b** Surface rendering of the complex, showing YheS, A- and P-tRNAs, mRNA, and the SecM nascent chain. The 70S ribosome is displayed as a transparent surface. **c** Close-up view of the nascent SecM chain attached to the P-tRNA. Only the C-terminal three residues (Arg163–Ala164–Gly165) are resolved. Cryo-EM density is shown as a mesh. The map without sharpening is used. **d**, **e** Overall structure and domain composition of YheS. The two nucleotide-binding domains (NBD1 and NBD2) are connected by the P-tRNA-interaction Motif (PtIM). Two bound ATP molecules are shown as spheres. **f, g** Detailed views of the ATP-binding sites in YheS. Mg^{2+} ions are coordinated at both sites. ATP molecules are located at the interface between NBD1 **f** and NBD2 **g**.

CP normally interacts with the elbow of the P-tRNA (Supplementary Fig. 7b), this CP shift is likely related to the P-tRNA relocation induced by YheS, as described below. These shifts in the SSU head and the LSU CP eliminate their inter-subunit contacts, particularly those between uS13 (SSU) and uL5/bL31 (LSU), resulting in a spatial gap in this region (Supplementary Fig. 7a).

PtIM interactions with the 23S rRNA

YheS establishes extensive contacts with domain V of the 23S rRNA near the PTC (Fig. 2e, f, Supplementary Table 3). Specifically, ten residues located at the tip of PtIM (His258, Arg267, Thr271, Lys274, Gln275, Gln277, Ser278, Arg279, Lys281, and Arg285) form hydrogen bonds or salt bridges with the nucleotides in helices 74, 75, 80, and 93 of domain V. These interactions anchor PtIM firmly to the LSU and define its position relative to the PTC. A comparison with the SecM-arrested 70S ribosome in the absence of YheS reveals that the overall conformation of the 23S rRNA near the PTC remains largely unchanged, except for several tunnel-lining nucleotides (A2062, U2506, U2585) (Supplementary Fig. 7c), as well as A2602 in helix H93 (Supplementary Fig. 7d). Specifically, A2062 and U2506 change their base orientations, U2585 moves outward from the exit tunnel, and A2602 adopts a flipped-in conformation. These movements appear to result from the shifted acceptor arm of the P-tRNA, as described below.

P-tRNA interaction and relocation

YheS interacts with the P-tRNA at multiple regions, contributing to its relocation. In NBD2, Gln408 forms hydrogen bonds with nucleotide C56 of the P-tRNA, and Arg411 stacks onto the base via a π-interaction (Fig. 2g). In parallel, Asp412 and Gly421 form hydrogen bonds with G19. YheS also binds to the 3′ region of the P-tRNA. Lys269 and Ala270, located at the tip of PtIM, form a salt bridge with U73 and a hydrogen bond with C74, respectively (Fig. 2h, Supplementary Table 4).

Compared to the SecM-arrested ribosome without YheS, the position of the P-tRNA acceptor arm is drastically altered (Fig. 2i). The tip of PtIM occupies the canonical location of nucleotides 71–74 in the acceptor arm. Notably, the position of PtIM is stabilized by multiple interactions with the 23S rRNA (Fig. 2e, f). As a result, the P-tRNA acceptor stem is displaced by 5–12 Å (measured using the P atoms of the phosphate groups) (Fig. 2i), disrupting the base pair between C75 of the P-tRNA and Gm2251 of the 23S rRNA (Supplementary Fig. 7d). In parallel, the elbow region of the P-tRNA rotates by ~25° (Fig. 2i), likely due to the interaction between YheS and the P-tRNA elbow. This rotation also alters the interaction with the CP: in the SecM-arrested ribosome without YheS, Arg80 of uL5 stacks with the elbow of the P-tRNA, but this interaction is lost in the YheS-bound complex (Supplementary Fig. 7b). Instead, Arg80 forms salt bridges with the phosphate groups of Ψ55 and G57 of the P-tRNA (Supplementary Fig. 7b). This change arises from both the P-tRNA rotation and the CP displacement induced by YheS binding.

SecM nascent chain relocation

As consequences of these P-tRNA rearrangements, the 3′-terminal A76 of the P-tRNA is shifted outward by 2.2 Å from the PTC (measured using the O3′ atoms) (Fig. 2i, j), thereby mechanically coupling the

https://doi.org/10.1038/s41467-026-72863-1

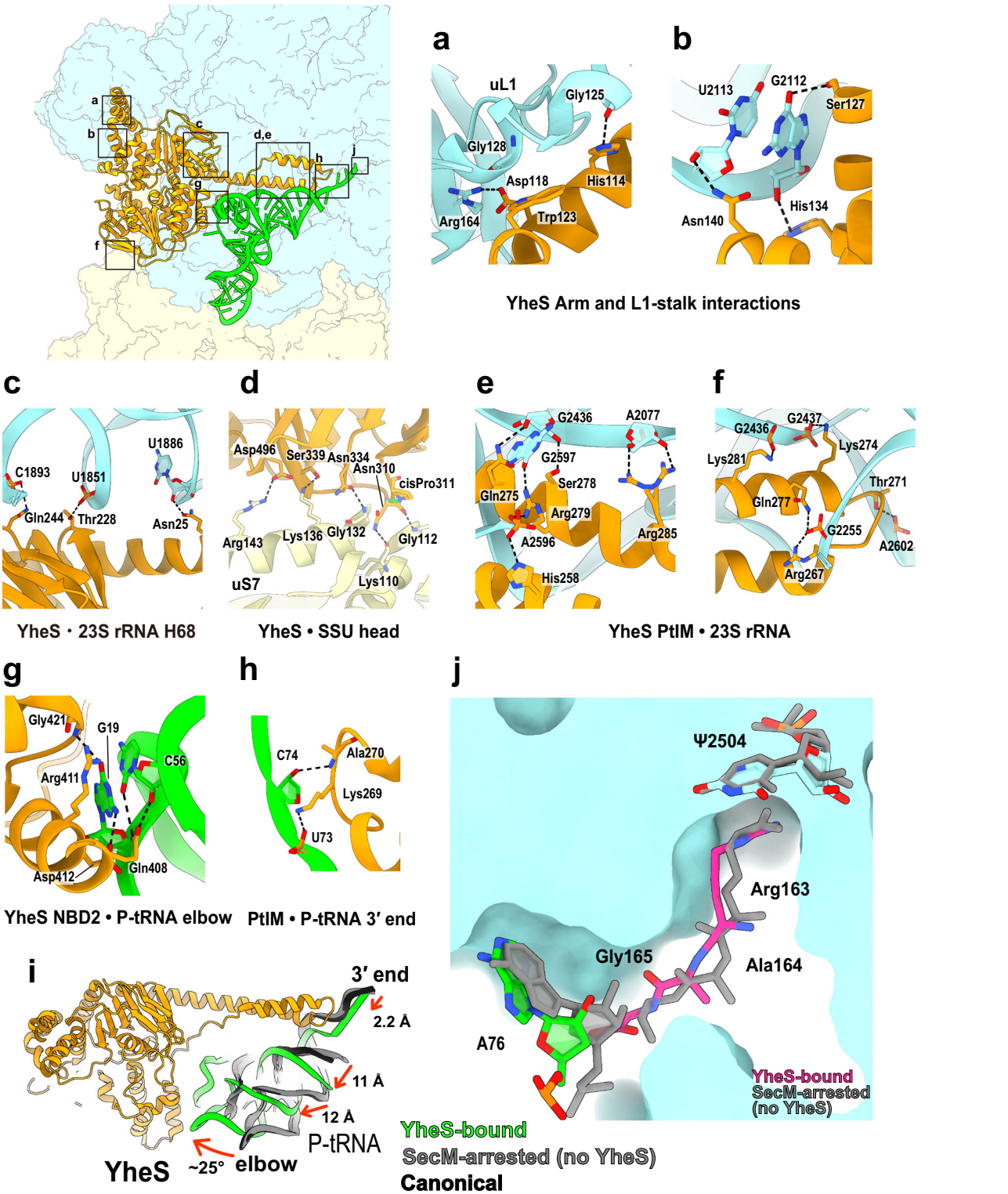

Fig. 2 | YheS interactions with the ribosome and P-tRNA. a, b The Arm subdomain of YheS interacts with both the protein (uL1, **a**) and RNA (helix H76 of 23S rRNA, **b**) components of the L1-stalk. **c** The residues at the base of PtIM form multiple polar interactions with the 23S rRNA near the L1-stalk. **d** NBD1 of YheS interacts with ribosomal protein uS7 in the SSU head. **e, f** PtIM of YheS forms multiple polar interactions with the 23S rRNA near the PTC. **g, h** Interactions between YheS and P-tRNA. NBD2 of YheS forms hydrogen bonds and stacking interactions with the P-tRNA elbow **g**, while the tip of PtIM forms two hydrogen bonds with the 3′ end of the P-tRNA **h. i** Relocation of the P-tRNA upon YheS binding. The P-tRNA in the present complex with YheS is colored green, while that of the SecM-arrested ribosome without YheS and that of the canonical elongating ribosome (PDB: 8B0X)[45] are shown in gray and black, respectively. **j** Conformational comparison of the P-tRNA and SecM nascent chain between the SecM-arrested ribosome with or without YheS. In the YheS-bound state, the 3′ end of the P-tRNA and the attached SecM nascent chain are retracted by ~2 Å toward the tunnel entrance.

P-tRNA displacement to the SecM nascent chain. The density for the SecM nascent chain is weak, and only the C-terminal three residues (Arg163-Ala164-Gly165) can be traced (Fig. 1c and Supplementary Fig. 5c). Relative to the SecM-arrested ribosome without YheS, these three residues are shifted by 1.1, 1.7, and 1.6 Å, respectively (measured by using their C_α atoms) (Fig. 2j). Although the π stacking between the Arg163 side chain and the 23S rRNA Ψ2504 is preserved, the Arg163 side-chain conformation is altered (Fig. 2j). These findings collectively suggest that YheS binding relocates the P-tRNA along with the attached SecM nascent chain, thereby likely perturbing the interactions required for translation arrest [27].

In the SecM-arrested ribosome without YheS, the amino group of the A-site Pro166 forms hydrogen bonds with the carbonyl group of SecM Ala164 and the 3′-OH group of the P-tRNA (Supplementary Fig. 5d). These interactions are reportedly the key arresting mechanism that prevents the nucleophilic attack of the Pro166 amino group on the ester bond between Gly165 and P-tRNA[27]. On the other hand, in the YheS-bound structure, the density of Pro166 is extended and not clearly connected to the A-tRNA 3′-terminus (Fig. 1c), suggesting weakening of these interactions. This agrees with the measured distances from the amino-group N atom of Pro166 to the carbonyl O atom of Ala164 and to the O3′ atom of the P-tRNA A76 (3.7 and 4.5 Å, respectively), both of which exceed typical hydrogen bonding distance (2.5-3.5 Å).

However, despite the loss of arresting interactions, the Pro166 amino group remained too far away from the P-tRNA-Gly165 ester bond (5.5 Å between the amino N atom of Pro166 and the carbonyl C atom of Gly165), compared with the non-arrested structures (3.0-3.2 Å, PDB IDs: 8CVJ and 8CVL)[46]. This indicates that the dissociation of YheS is required for catalytic geometry to be restored, consistent with our previous biochemical observations[40].

Mutational analysis of YheS–ribosome and tRNA interactions

To evaluate the functional significance of the YheS interactions with the ribosome and P-tRNA, we introduced a series of point mutations into YheS and measured their ability to release SecM-arrested ribosomes (Fig. 3). The activity of each YheS mutant in *E. coli* cells was measured using *sfGFP-secM* (E134-R168)-*lacZ* reporter, which enables analysis of arrest release independently of SecA-mediated pulling force[40,48,49]. Notably, the single-point substitutions D118A and W123A, which disrupt the interactions with the ribosomal protein uL1, and R279A, targeting the 23S rRNA near the PTC, each led to a greater than 50% reduction in activity (Fig. 3a and f). The corresponding multi-point mutants, H114A/D118A/W123A and Q275A/Q277A/R279A/K281A, exhibited even more severe defects, supporting the importance of these contact sites. In contrast, mutations targeting YheS interactions with more distal regions of the 23S rRNA or with uS7 in the SSU resulted in minor reductions in activity (Fig. 3b, c, and g). These findings suggest that the direct contacts with the protein components of the L1-stalk and with the 23S rRNA adjacent to the PTC affect the YheS function.

Mutations disrupting YheS interactions with the P-tRNA, whether targeting the elbow region or the 3′ acceptor arm, had only modest effects on its activity (Fig. 3d, e). This indicates that while YheS interacts with the P-tRNA, these interactions are auxiliary, and the primary mechanism of action relies on the ribosome binding. These results, together with the structural observations, support a model in which YheS binds to the E site through interactions with uL1 and inserts its PtIM near the PTC, thereby displacing the acceptor arm of the P-tRNA along with the attached SecM nascent chain.

Behavior of SecM during P-tRNA relocation in molecular simulations

To explore how the YheS-induced relocation of P-tRNA affects the tethered SecM nascent chain, we performed steered molecular dynamics (SMD) simulations focusing on the SecM segment within the ribosomal tunnel. Simulations were initiated from a deliberately reduced model extracted from the previously reported SecM-arrested ribosome[27]. In this setup, only the SecM segment (residues 149–165) and selected surrounding 23S rRNA fragments within the tunnel were retained, while the remainder of the ribosome, including the A- and P-tRNA and distal rRNA regions, was omitted to limit system size.

Within this reduced system, SecM residues 149–165 were subjected to extensions approximating the displacement observed in our cryo-EM structure (Supplementary Fig. 8a-d). In the simulations, we did not observe pronounced conformational destabilization within the portion of the α-helical region (Thr152–Ile156) under the tested conditions (Supplementary Fig. 9). However, increases in inter-residue distances and changes in dihedral angles were observed in several intra- and intermolecular interactions (e.g., Ile156–Ile162 and Arg163–Ψ2504) (Supplementary Fig. 8e and 9). These contacts have previously been implicated in SecM-mediated translational arrest through structural observation[27] and mutational analyses[11]. Given the reduced ribosomal context and timescale, these observations should be interpreted qualitatively. Nevertheless, they provide exploratory support for the possibility that structural rearrangements associated with P-tRNA relocation could weaken key peptide–tunnel interactions linked to translation arrest.

Comparison with other ABCF proteins

The key structural difference between antibiotic resistance (ARE) ABCFs and non-ARE ABCFs lies in the length of their PtIM (Supplementary Fig. 10). In the ARE ABCF-ribosome complexes, the long PtIM extends into the peptidyl transferase center (PTC) and even the exit tunnel, displacing antibiotics bound within the tunnel (Supplementary Fig. 10b)[31–35]. Accordingly, ARE-ABCFs with long PtIMs are unable to function when a nascent chain occupies the exit tunnel and are thought to act only when the initiator tRNA is accommodated (Supplementary Fig. 10b). In contrast, non-ARE ABCFs such as *E. coli* EttA possess short PtIMs that do not reach the PTC[37] (Supplementary Fig. 10c). These ABCFs induce only minor rRNA rearrangements or subtle shifts in the P-tRNA but help stabilize the P-tRNA to promote efficient peptidyl transfer [38].

Interestingly, in our YheS-ribosome structure, the P-tRNA is relocated more substantially than in other non-ARE ABCF complexes, resembling the extent seen with ARE-ABCFs (Supplementary Fig. 10), despite the short PtIM of YheS. Since the SecM nascent chain occupies the exit tunnel, YheS likely induces P-tRNA relocation that may alter interactions within the tunnel. This is achieved via extensive contacts between PtIM and the 23S rRNA near the PTC (Fig. 2e and f), combined with contacts at the tRNA elbow that rotate the P-tRNA toward the E site (Fig. 2g).

Finally, ATP hydrolysis likely triggers conformational changes at the NBD1–NBD2 interface, disrupting the interdomain interactions mediated by the γ-phosphate groups (Fig. 1d–g). These changes would render YheS incompatible with the E-site architecture and promote its dissociation. Upon YheS release, the P-tRNA can be relocated correctly, allowing translation to resume its normal cycle (Fig. 4).

Discussion

In this study, we determined the 2.82 Å structure of YheS in complex with the ribosome arrested by the SecM nascent chain. The structure revealed multiple contact points, and the mutational analysis highlighted the importance of the Arm and PtIM of YheS, which interact with the L1-stalk and the 23S rRNA near the PTC. These interactions displace the CCA end of the P-tRNA and retract the SecM nascent chain by approximately 2 Å (based on the C_α positions of A164 and Gly165). Importantly, density for residues N-terminal to Arg163 is largely absent, suggesting reduced stabilization of intratunnel contacts upon

https://doi.org/10.1038/s41467-026-72863-1

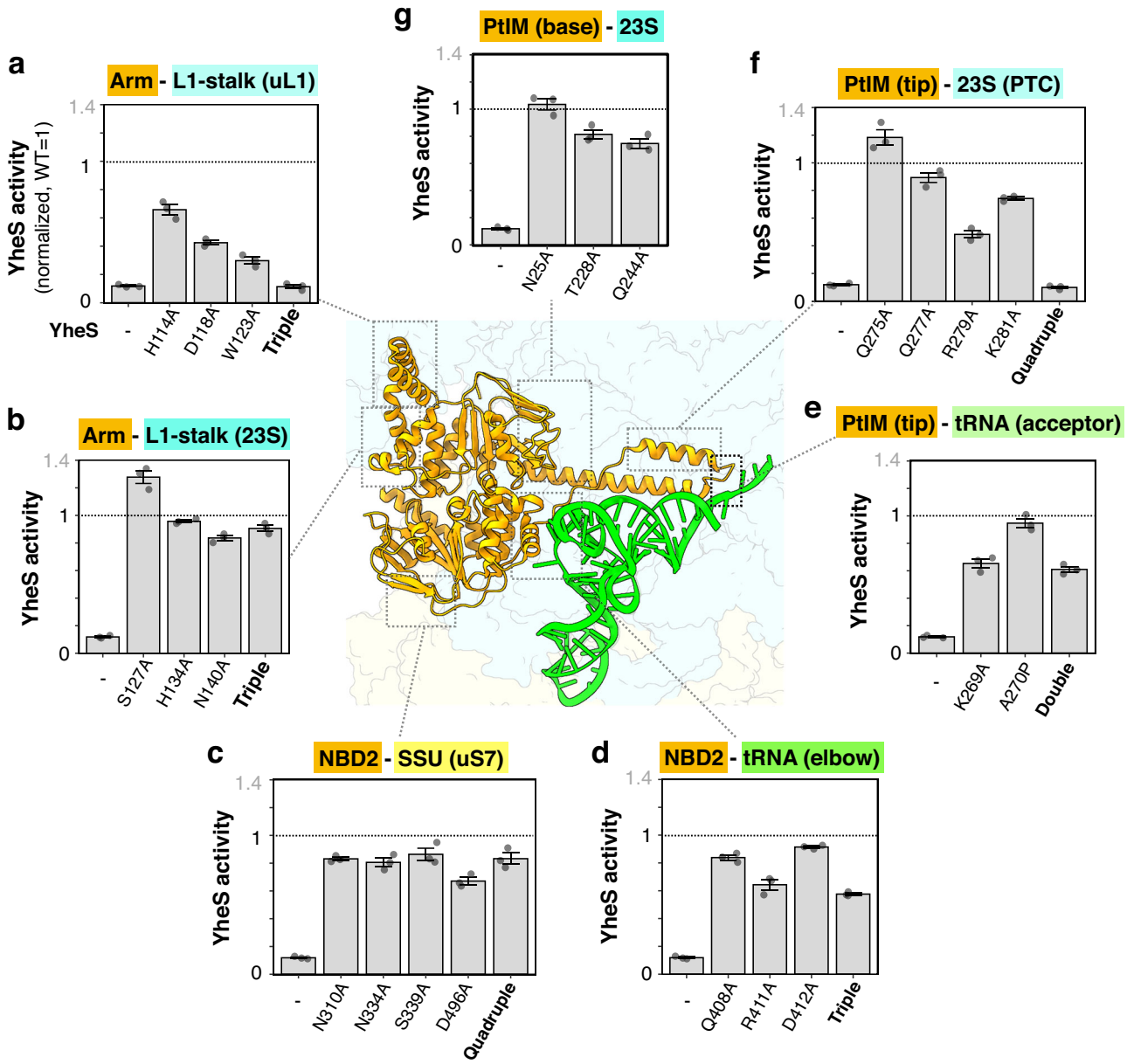

Fig. 3 | Mutational analysis of YheS residues. Alanine or proline substitutions were introduced into YheS residues that mediate interactions with the ribosome or P-tRNA, either individually or in combination. The arrest-releasing activity of each mutant was quantified as described in the Methods and normalized to wild-type YheS (set to 1). The mean ± SE estimated from three independent biological replicates ($n = 3$) is shown. Source data are provided as a Source Data file. **a** The Arm-uL1 interaction in the L1-stalk (H114A, D118A, W123A, triple mutant). **b** The Arm-rRNA interaction in the L1-stalk (S127A, H134A, N140A, triple mutant). **c** NBD1-uS7 interaction in the SSU head (N310A, N334A, S339A, D496A, quadruple mutant). **d** NBD2 residues contacting the P-tRNA elbow (Q408A, R411A, D412A, triple mutant). **e** The PtIM tip contacting the P-tRNA acceptor arm (K269A, A270P, double mutant). **f** The PtIM tip contacting 23S rRNA near the PTC (Q275A, Q277A, R279A, K281A, quadruple mutant). **g** The base of PtIM contacting 23S rRNA near the L1-stalk (N25A, T228A, Q244A).

YheS binding. In contrast, both the previously reported structure and our structure of the SecM-arrested ribosome without YheS showed that the SecM nascent chain remains stably folded throughout the exit tunnel ([27]; Supplementary Fig. 5b).

Notably, in the SecM Glu134–Leu169 construct used in this study, the nascent chain adopts interactions with the ribosomal exit tunnel comparable to those observed in the full-length SecM structure[27]. This comparison indicates that the truncated construct faithfully recapitulates the arrested state prior to YheS binding. While the overall ribosome architecture remains largely unchanged between the YheS-free and YheS-bound states, pronounced rearrangements are observed in the P-tRNA and the attached nascent chain. The direct structural comparison between these two states provides key insights into how YheS binding remodels the arrest complex and thereby contributes to release of translation stalling.

A previous study demonstrated that SecM-induced arrest relies on cumulative interactions between the nascent chain and the exit tunnel, including an α-helix formed downstream of Phe150 and the stacking interaction between Arg163 and Ψ2504[27]. These interactions stabilize Ala164 and facilitate hydrogen bonding with the incoming Pro166 at the A site, thereby inhibiting peptidyl transfer. Mutagenesis has validated the functional importance of these residues[11]. Although Ile156 and Ile162 have also been highlighted, their precise roles remain unclear because they do not directly contact the ribosome. In our cryo-EM structure, relocation of the P-tRNA is accompanied by a shift of the SecM C-terminal segment, suggesting potential perturbation of these

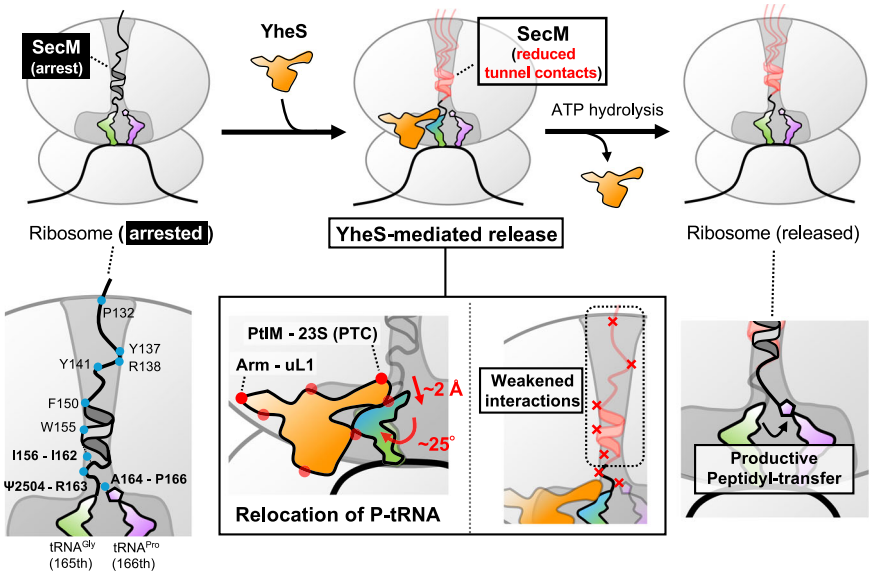

Fig. 4 | Proposed model for YheS-mediated release of SecM-arrested ribosome. Schematic representation of the structural rearrangements observed upon YheS binding. In the arrested state, the SecM nascent chain forms extensive interactions throughout the exit tunnel. YheS binds to the vacant E site and induces relocation of the P-tRNA, accompanied by a shift of the attached nascent chain. These rearrangements are expected to weaken arrest-associated interactions within the ribosomal exit tunnel and near the peptidyl transferase center. Subsequent ATP hydrolysis is expected to promote a conformational change of YheS, leading to its dissociation and facilitating restoration of productive translation at the PTC.

arrest-related contacts. Consistent with this structural observation, MD simulations performed under simplified conditions showed transient weakening or loss of interactions such as Ile156–Ile162, and Arg163–Ψ2504. These observations qualitatively align with previous genetic and structural data[11,27]. However, given the limited simulation timescale and reduced system size, the MD results should be interpreted cautiously and do not establish a quantitative displacement requirement. Further investigation will be necessary to rigorously evaluate the proposed model.

Based on our findings, we propose the following model for YheS-mediated release (Fig. 4)

1. Recognition: YheS binds to the vacant E site via the L1-stalk.
2. Insertion: PtIM of YheS relocates the P-tRNA and forms stable contacts with the 23S rRNA.
3. Disruption: This P-tRNA relocation shifts the attached SecM nascent chain, potentially weakening key arrest-related interactions (including the Ala164-Pro166 geometry and tunnel contacts such as Ile156-Ile162 and Arg163-Ψ2504).
4. Dissociation: ATP hydrolysis triggers conformational changes in YheS, promoting its dissociation from the ribosome, allowing peptidyl transfer to continue the nascent chain elongation.
5. This model may explain why YheS is ineffective against other arrest peptides, such as the RAPP motif in *S. medicae* ApdP[40]. While ApdP arrests the ribosome through an identical mechanism involving the penultimate alanine and the A-site proline[50], it relies more heavily on PTC-proximal residues and less on extended tunnel contacts[16]. Therefore, YheS, which potentially disrupts interactions within the tunnel, may be ineffective at releasing ApdP-induced arrest. Alternatively, the stalling structure of the RAPP motif may be rapidly reconstructed after YheS dissociates.

While translation factors like EF-P (eIF5A) and EttA promote elongation by stabilizing the P-tRNA from the E site[37,38,51], YheS acts by reshaping the interactions of the nascent chain within the exit tunnel. This action is also distinct from the ARE-ABCFs, which directly dislodge antibiotics from the tunnel[31–35]. These findings underscore how different ABCF proteins resolve diverse translational defects via specialized mechanisms[31–35,39–42,52]. Moreover, the actions of YheS contrast with the external pulling force of the Sec translocon, yet both effectively relieve SecM-induced arrest, highlighting the mechanistic versatility in arrest resolution [26,53–55].

Finally, our results provide a structural framework with mechanistic implications for understanding how YheS resolves SecM-induced stalling. Recently, several structures of *E. coli* ABCF-bound ribosomes, including YheS in the absence of SecM, have been documented[56]. However, because these complexes lack a nascent chain within the exit tunnel, they do not directly inform on the mechanism of SecM arrest release. The preprint further proposed that YheS binding may alter the positioning of the P-tRNA relative to the peptidyl transferase center. While that model emphasizes modulation of catalytic geometry, our findings highlight additional rearrangements of arrest-associated interactions. These perspectives are not mutually exclusive and may reflect complementary aspects of YheS-mediated rescue. Together, our study advances the understanding of ABCF functional specialization and provides a foundation for future efforts to engineer translation regulators tailored to specific sequence or structural contexts.

Methods

E. coli strains, plasmids, and oligonucleotides

E. coli strain BW25113 {Δ(*araD-araB*)567, Δ*lacZ4787*(::*rrnB*−3), λ-, *rph*−1, Δ(*rhaD-rhaB*)568, *hsdR514*} was used as the experimental standard strain. Plasmids and oligonucleotides used in this study are listed in Supplementary Table 5 and 6, respectively. Plasmids were constructed using standard cloning procedures, including Gibson assembly and site-directed mutagenesis. The sequence files of the plasmids constructed in this study are available in the Mendeley repository [doi: 10.17632/5cjmw3wmp8.1].

In vitro translation

The coupled in vitro transcription-translation reaction was performed using PURE*frex* v1.0 (GeneFrontier), as described previously[10,57]. The DNA template encoding the SecM arrest peptide was PCR-amplified from pCY3867 (pCA24N carrying *folA_60aa-secM*(E134-L169)-*lacZa*), using primer 1 (GGCCTAATACGACTCACTATAGGAGAAATCATAAAAAATTTATTTGCTTTGTGAGCGG) and primer 3

(AGTCAGTCACGATGAATTCCCCTAGCTTGG). Following an incubation at 37 °C for 30 min, the reaction mixture was treated with purified YheS-EQ$_2$ at a final concentration of 5 μM and incubated for an additional 10 min. The mixture was then placed on ice and immediately used for cryo-EM grid preparation. For analysis of translational products, in vitro translation was performed in the presence of Cy5-Met-tRNA^{fMet} at 37 °C for 30 min. The reaction was stopped by adding excessive amount of 5% TCA, and the precipitated material was washed with ice-cold acetone and dissolved in SDS sample buffer (62.5 mM Tris-HCl, pH 6.8, 2% SDS, 10% glycerol, 50 mM DTT) that had been treated with RNAsecure (Ambion). The sample was then divided into two portions, one of which was incubated with 50 μg /ml of RNase A (Promega) at 37 °C for 30 min, and separated by a WIDE Range SDS-PAGE system (Nakalai Tesque). Fluorescent signals were visualized on an iBright FL1500 imager (Thermo Fisher Scientific) using the EX3 excitation filter (608–632 nm) and EM3 emission filter (675–720 nm).

Purification of wild type YheS and YheS-EQ$_2$ proteins

E. coli BL21 (DE3) cells harboring pCY3857 or pCY3863, which encodes N-terminally His$_6$-tagged YheS or YheS-EQ$_2$ respectively, were grown overnight at 37 °C in LB medium supplemented with 100 μg/ml ampicillin. The next day, the overnight culture was diluted into fresh LB medium containing 100 μg/ml ampicillin and grown at 37 °C until the A_{600} reached 0.6. Protein expression was induced by adding 0.05% arabinose, followed by incubation for an additional 2 h at 37 °C. Cells were harvested by centrifugation at 5,000 × g for 15 min at 4 °C.

Cell pellets were washed and resuspended in disruption buffer (20 mM Tris-HCl, pH 7.5, 500 mM NaCl, 10% glycerol, 7 mM β-ME, 10 mM imidazole, EDTA-free cOmplete™ mini protease inhibitor cocktail). Cells were disrupted by sonication, and debris was removed by ultracentrifugation (100,000 × g, 40 min at 4 °C). The recovered lysate was loaded onto a column filled with Ni-NTA Superflow resin (QIAGEN). After washing the column with ten column volumes of wash buffer {20 mM Tris-HCl, pH 7.5, 500 mM NaCl, 10% glycerol, 7 mM β-ME, 20 mM imidazole}, the YheS-EQ$_2$ protein was eluted by wash buffer containing steps of 50, 100, and 300 mM imidazole. The fraction containing YheS or YheS-EQ$_2$ was concentrated using an Amicon Ultra 30 kDa filter (Merck) and solvent exchanged on a PD-10 column (Cytiva) to storage buffer (20 mM Tris-HCl, pH 7.5, 150 mM NaCl, 10% glycerol, 7 mM β-ME). The purified proteins were stored at −80 °C.

Grid preparation and cryo-EM data acquisition

For the cryo-EM analysis, 3 μL of the PURE system reaction solution containing stalled ribosomes was applied onto a glow-discharged holey-carbon grid coated with a continuous 2 nm-thick carbon film (Quantifoil Au 300 mesh, R2/1 + 2 nm Ultra-Thin Carbon Film) and incubated for 30 s in a controlled environment of 100% humidity at 4 °C. The grids were blotted for 4 s, and then plunge frozen in liquid ethane, using a Vitrobot Mark IV (FEI). The datasets were collected using a Titan Krios G4 microscope (Thermo Fisher Scientific), running at 300 kV and equipped with a Gatan Quantum-LS Energy Filter (GIF). A Gatan K3 Summit direct-electron detector was used at a pixel size of 0.83 Å (magnification of ×105,000) with an exposure of approximately 30 electrons per Å^2 with 30 movie frames. The data were automatically acquired using the EPU software (Thermo Fisher Scientific), with a defocus range of −0.8 to −2.0 μm, and 18,200 movies were obtained.

Cryo-EM image processing

The data were processed with cryoSPARC[58] and RELION[59]. In cryoSPARC, the dose-fractionated movies were subjected to beam-induced motion correction and dose weighting using patch motion correction, and the contrast transfer function (CTF) parameters were estimated using patch-based CTF estimation. From the 18,200 preprocessed micrographs, 1,770,974 particles were automatically picked by the template picker, using the references created by the blob picker and several rounds of 2D classification. An ab-initio structure was reconstructed and subjected to heterogeneous refinement (680,146 particles). Afterward, 675,529 particles were selected and subjected to NU refinement. The particles were transferred to RELION, and 3D refinement, CTF refinement, and Bayesian polishing were performed. The particles were then subjected to non-align local-masked 3D classification, using a focus mask covering YheS and the L1-stalk, and thus separated based on with and without YheS bound, which were 520,241 and 148,052 particles, respectively.

The particles with YheS were further subjected to non-align local-masked 3D classification using a mask covering the A- and P-tRNAs. Then, 390,797 particles with the tRNAs were selected and reprocessed with cryoSPARC and further subjected to non-align masked 3D classification, using a mask covering SSU and A-tRNA, resulting in the 3D classes with different SSU orientations against LSU. One class with 131,767 particles was selected. To improve the occupancy of the factors, the particles were further subjected to non-align local-masked 3D classification, covering the A-tRNA. Afterward, 64,373 particles with A-tRNA were further subjected to non-align local-masked 3D classification, using a mask covering the A-tRNA, P-tRNA, YheS, and L1-stalk. After 50,797 particles were selected, they were subjected to NU refinement, resulting in the final map of the SecM-arrested ribosome with YheS at 2.82 Å resolution.

To improve the local resolution, local-masked 3D refinements were performed using masks covering the SSU head, SSU body, LSU, and YheS with L1-stalk. The NU refined map and the local refined maps were subjected to *B*-factor sharpening and local resolution filtering. For further model building and model refinement, these maps were combined into a composite map by aligning the local-refined maps to the NU refined map in Chimera[60] by using the 'fitmap' command without scaling, followed by performing the 'vop maximum' command to adopt the largest values pointwise among the maps. This composite map was further upsampled to a smaller pixel size (0.666 Å/pix) by using Phenix v1.20[61] and *Coot* 0.8[62]. The composite map using the maps without sharpening, local-resolution filtering, or upsampling was also made.

The 148,052 particles without YheS from the first local-masked 3D classification were reprocessed with cryoSPARC, and subjected to non-align masked 3D classification, using a mask covering SSU. The class with relatively clear SecM density was selected (26,202 particles), followed by a non-align local-masked 3D classification, covering the A- and P-tRNAs. The 26,202 particles with A- and P-tRNAs were subjected to NU refinement, resulting in the final map of the SecM-arrested ribosome without YheS at 2.89 Å resolution. This map was also subjected to *B*-factor sharpening and local resolution filtering, followed by upsampling to a smaller pixel size (0.719 Å/pix). No composite map was made for this map.

Model building and refinement

The reported *E. coli* ribosome structures, PDB IDs: 8QOA[27] and 8B0X[45], were used for the starting models of the RNA and protein parts, respectively. The YheS model was obtained by AlphaFold2[63]. The mRNA, tRNA, ATP, and nascent chain models were built manually. Manual revision was done using *Coot* 0.8[62]. Alternative conformations supported by the density were introduced. Geometrical restraints of modified residues and ligands were calculated by Grade Web Server (http://grade.globalphasing.org). The models were then refined by using Phenix.real_space_refine v1.20[61]. Global energy minimization with rotamer and Ramachandran restraints was done against the map with *B*-factor sharpening,local-resolution filtering, and upsampling. Following ADP refinement was done against the map without sharpening. Validation was performed by MolProbity[64]. The statistics are listed in Supplementary Table 1. ChimeraX[65] was used for making figures.

β-galactosidase assay

E. coli cells harboring both pCY2524 {GFP-*secM* (E134-R168)-*lacZ*reporter} and the YheS-expressing plasmid were grown overnight at 37 °C in LB medium, supplemented with 100 μg/ml ampicillin and 20 μg/ml chloramphenicol. On the next day, they were inoculated into fresh LB medium containing 0.002% arabinose, 100 μg/ml ampicillin, and 20 μg/ml chloramphenicol and grown at 37 °C. Expression of YheS or its derivatives was induced by the addition of 100 μM IPTG when the A_{660} reached 0.2. After further incubation (A_{660} = ~0.6), 20 μl portions were subjected to a β-galactosidase assay as described previously [10,40].

Molecular simulation

To reduce system size, we constructed a truncated model consisting of SecM residues 149–165 and nearby 23S rRNA fragments, excluding the A- and P-tRNAs as well as the remainder of the ribosome. The cryo-EM structure of the SecM-arrested ribosome was obtained from the Protein Data Bank (PDB: 8QOA), representing the SecM-arrested ribosome without YheS[27]. To investigate the dynamics of SecM extension toward the C-terminus, we extracted the LSU RNAs within 10 Å of SecM (residues 149-165) and considered their connections, leaving a total of nine RNA strands (residues 745-752, 783-792, 1779-1783, 2055-2071, 2251-2253, 2438-2453, 2500-2507, 2572-2588, 2599-2612, where these residues practically encompass the space up to a distance of 16 Å from Gly165). This structure of SecM with the surrounding RNA was solvated, and counterions were added to maintain electroneutrality, resulting in a system of 67,829 total atoms (including 21,434 water molecules and 87 K^+ ions) in a 96.4×90.5×94.7 $Å^3$ box. The resulting system was subjected to 300-step energy minimization followed by 500-ps NVT and 500-ps NPT equilibration with heavy atom restraints. The force field parameters used were Amber ff19SB for proteins/peptides, TIP3P for water molecules, OL3 for RNA, and modrna08 for modified nucleosides. The temperature and pressure were regulated by the Berendsen (weak-coupling) thermostat and barostat (300 K and 1 bar, respectively). The equilibrated system was then subjected to subsequent steered molecular dynamics (SMD) simulations. In SMD simulations, the distance between N-terminal Lys (C_α) and C-terminal Gly165 (C_α) atoms was extended by 2, 5, or 10 Å by applying a harmonic potential (with a force constant of 12 kcal·mol^{-1}·$Å^{-2}$) while keeping the N-terminal Lys149 backbone fixed. Three independent 100-ns SMD trajectories were generated for each extension. Throughout the SMD, the RNA backbone was restrained to maintain the ribosomal LSU conformation. All molecular dynamics simulations were performed using the Amber 24 package[66].

Reporting summary

Further information on research design is available in the Nature Portfolio Reporting Summary linked to this article.

Data availability

The atomic coordinates generated in this study have been deposited in the Protein Data Bank (PDB) under the accession codes 9VVI and 9XWO. The cryo-EM density maps of the composite map and the raw maps have been deposited in the Electron Microscopy Data Bank (EMDB) under the accession codes EMD-65381, EMD-66482, EMD-66483, EMD-66484, EMD-66485, EMD-66486, and EMD-67339. The sequence files of the plasmids constructed in this study are available in the Mendeley repository [doi: 10.17632/5cjmw3wmp8.1]. Molecular dynamics simulations initial coordinate and simulation input files and a coordinate file of the final output are provided as Figshare repository entry 30155464. Source data are provided with this paper.

References

1. Ito, K. & Chiba, S. Arrest Peptides: Cis-Acting Modulators of Translation. *Annu. Rev. Biochem.* **82**, 171–202 (2013).
2. Höpfler, M. & Hegde, R. S. Control of mRNA fate by its encoded nascent polypeptide. *Mol. Cell* **83**, 2840–2855 (2023).
3. Chiba, S., Fujiwara, K., Chadani, Y. & Taguchi, H. Nascent chain-mediated translation regulation in bacteria: translation arrest and intrinsic ribosome destabilization. *J. Biochem.* **173**, 227–236 (2023).
4. Ude, S. et al. Translation Elongation Factor EF-P Alleviates Ribosome Stalling at Polyproline Stretches. *Science* **339**, 82–85 (2013).
5. Doerfel, L. K. et al. EF-P Is Essential for Rapid Synthesis of Proteins Containing Consecutive Proline Residues. *Science* **339**, 85–88 (2013).
6. Dimitrova, L. N., Kuroha, K., Tatematsu, T. & Inada, T. Nascent Peptide-dependent Translation Arrest Leads to Not4p-mediated Protein Degradation by the Proteasome. *J. Biol. Chem.* **284**, 10343–10352 (2009).
7. Lu, J., Hua, Z., Kobertz, W. R. & Deutsch, C. Nascent Peptide Side Chains Induce Rearrangements in Distinct Locations of the Ribosomal Tunnel. *J. Mol. Biol.* **411**, 499–510 (2011).
8. Mizuno, M. et al. The nascent polypeptide in the 60S subunit determines the Rqc2-dependency of ribosomal quality control. *Nucleic Acids Res.* **49**, 2102–2113 (2021).
9. Lu, J. & Deutsch, C. Electrostatics in the Ribosomal Tunnel Modulate Chain Elongation Rates. *J. Mol. Biol.* **384**, 73–86 (2008).
10. Chadani, Y. et al. Intrinsic Ribosome Destabilization Underlies Translation and Provides an Organism with a Strategy of Environmental Sensing. *Mol. Cell* **68**, 528–539.e5 (2017).
11. Nakatogawa, H. & Ito, K. The Ribosomal Exit Tunnel Functions as a Discriminating Gate. *Cell* **108**, 629–636 (2002).
12. Gong, F. & Yanofsky, C. Instruction of Translating Ribosome by Nascent Peptide. *Science* **297**, 1864–1867 (2002).
13. Onouchi, H. et al. Nascent peptide-mediated translation elongation arrest coupled with mRNA degradation in the *CGS1* gene of *Arabidopsis*. *Gene. Dev.* **19**, 1799–1810 (2005).
14. Chiba, S., Lamsa, A. & Pogliano, K. A ribosome-nascent chain sensor of membrane protein biogenesis in *Bacillus subtilis*. *EMBO J.* **28**, 3461–3475 (2009).
15. Yanagitani, K., Kimata, Y., Kadokura, H. & Kohno, K. Translational Pausing Ensures Membrane Targeting and Cytoplasmic Splicing of *XBP1u* mRNA. *Science* **331**, 586–589 (2011).
16. Sakiyama, K., Shimokawa-Chiba, N., Fujiwara, K. & Chiba, S. Search for translation arrest peptides encoded upstream of genes for components of protein localization pathways. *Nucleic Acids Res* **49**, 1550–1566 (2021).
17. Adams, P. P. et al. Regulatory roles of *Escherichia coli* 5′ UTR and ORF-internal RNAs detected by 3′ end mapping. *eLife* **10**, e62438 (2021).
18. Fujiwara, K., Tsuji, N., Yoshida, M., Takada, H. & Chiba, S. Patchy and widespread distribution of bacterial translation arrest peptides associated with the protein localization machinery. *Nat. Commun.* **15**, 2711 (2024).
19. Ando, Y. et al. A mini-hairpin shaped nascent peptide blocks translation termination by a distinct mechanism. *Nat. Commun.* **16**, 2323 (2025).
20. Stein, K. C., Morales-Polanco, F., Lienden, J., van der, Rainbolt, T. K. & Frydman, J. Ageing exacerbates ribosome pausing to disrupt cotranslational proteostasis. *Nature* **601**, 637–642 (2022).
21. Chadani, Y. et al. Mechanistic dissection of premature translation termination induced by acidic residues-enriched nascent peptide. *Cell Rep.* **42**, 113569 (2023).
22. Nakatogawa, H. & Ito, K. Secretion Monitor, SecM, Undergoes Self-Translation Arrest in the Cytosol. *Mol. Cell* **7**, 185–192 (2001).
23. Murakami, A., Nakatogawa, H. & Ito, K. Translation arrest of SecM is essential for the basal and regulated expression of SecA. *Proc. Natl. Acad. Sci.* **101**, 12330–12335 (2004).

24. Muto, H., Nakatogawa, H. & Ito, K. Genetically Encoded but Non-polypeptide Prolyl-tRNA Functions in the A Site for SecM-Mediated Ribosomal Stall. *Mol. Cell* **22**, 545–552 (2006).
25. Woolhead, C. A., Johnson, A. E. & Bernstein, H. D. Translation Arrest Requires Two-Way Communication between a Nascent Polypeptide and the Ribosome. *Mol. Cell* **22**, 587–598 (2006).
26. Ito, K., Mori, H. & Chiba, S. Monitoring substrate enables real-time regulation of a protein localization pathway. *FEMS Microbiol. Lett.* **365**, fny109 (2018).
27. Gersteuer, F. et al. The SecM arrest peptide traps a pre-peptide bond formation state of the ribosome. *Nat. Commun.* **15**, 2431 (2024).
28. Gutierrez, E. et al. eIF5A Promotes Translation of Polyproline Motifs. *Mol. Cell* **51**, 35–45 (2013).
29. Murina, V. et al. ABCF ATPases Involved in Protein Synthesis, Ribosome Assembly and Antibiotic Resistance: Structural and Functional Diversification across the Tree of Life. *J. Mol. Biol.* **431**, 3568–3590 (2019).
30. Fostier, C. R. et al. ABC-F translation factors: from antibiotic resistance to immune response. *FEBS Lett.* **595**, 675–706 (2021).
31. Crowe-McAuliffe, C. et al. Structural basis for antibiotic resistance mediated by the *Bacillus subtilis* ABCF ATPase VmlR. *Proc. Natl. Acad. Sci.* **115**, 8978–8983 (2018).
32. Crowe-McAuliffe, C. et al. Structural basis of ABCF-mediated resistance to pleuromutilin, lincosamide, and streptogramin A antibiotics in Gram-positive pathogens. *Nat. Commun.* **12**, 3577 (2021).
33. Crowe-McAuliffe, C. et al. Structural basis for PoxtA-mediated resistance to phenicol and oxazolidinone antibiotics. *Nat. Commun.* **13**, 1860 (2022).
34. Mohamad, M. et al. Sal-type ABC-F proteins: intrinsic and common mediators of pleuromutilin resistance by target protection in staphylococci. *Nucleic Acids Res.* **50**, 2128–2142 (2022).
35. Obana, N. et al. Genome-encoded ABCF factors implicated in intrinsic antibiotic resistance in Gram-positive bacteria: VmlR2, Ard1 and CplR. *Nucleic Acids Res.* **51**, 4536–4554 (2023).
36. Boël, G. et al. The ABC-F protein EttA gates ribosome entry into the translation elongation cycle. *Nat. Struct. Mol. Biol.* **21**, 143–151 (2014).
37. Chen, B. et al. EttA regulates translation by binding the ribosomal E site and restricting ribosome-tRNA dynamics. *Nat. Struct. Mol. Biol.* **21**, 1–11 (2014).
38. Cui, Z. et al. Interplay between an ATP-binding cassette F protein and the ribosome from *Mycobacterium tuberculosis*. *Nat. Commun.* **13**, 432 (2022).
39. Hong, H.-R., Prince, C. R., Tetreault, D. D., Wu, L. & Feaga, H. A. YfmR is a translation factor that prevents ribosome stalling and cell death in the absence of EF-P. *Proc. Natl. Acad. Sci. USA* **121**, e2314437121 (2024).
40. Chadani, Y. et al. The ABCF proteins in *Escherichia coli* individually cope with 'hard-to-translate' nascent peptide sequences. *Nucleic Acids Res.* **52**, 5825–5840 (2024).
41. Takada, H., Fujiwara, K., Atkinson, G. C., Chiba, S. & Hauryliuk, V. Resolution of ribosomal stalling by EF-P and ABCF ATPases YfmR and YkpA/YbiT. *Nucleic Acids Res* **52**, 9854–9866 (2024).
42. Ousalem, F. et al. Global regulation via modulation of ribosome pausing by the ABC-F protein EttA. *Nat. Commun.* **15**, 6314 (2024).
43. Shimizu, Y. et al. Cell-free translation reconstituted with purified components. *Nat. Biotechnol.* **19**, 751–755 (2001).
44. Kobo, A., Taguchi, H. & Chadani, Y. Nonspecific N-terminal tetrapeptide insertions disrupt the translation arrest induced by ribosome-arresting peptide sequences. *J. Biol. Chem.* **300**, 107360 (2024).
45. Fromm, S. A. et al. The translating bacterial ribosome at 1.55 Å resolution generated by cryo-EM imaging services. *Nat. Commun.* **14**, 1095 (2023).
46. Syroegin, E. A., Aleksandrova, E. V. & Polikanov, Y. S. Insights into the ribosome function from the structures of non-arrested ribosome–nascent chain complexes. *Nat. Chem.* **15**, 143–153 (2023).
47. Qu, L. et al. Crystal Structure of ATP-Bound Human ABCF1 Demonstrates a Unique Conformation of ABC Proteins. *Structure* **26**, 1259–1265.e3 (2018).
48. Butkus, M. E., Prundeanu, L. B. & Oliver, D. B. Translocon "pulling" of nascent SecM controls the duration of its translational pause and secretion-responsive *secA* regulation. *J. Bacteriol.* **185**, 6719–6722 (2003).
49. Nakatogawa, H., Murakami, A. & Ito, K. Control of SecA and SecM translation by protein secretion. *Curr. Opin. Microbiol.* **7**, 145–150 (2004).
50. Morici, M. et al. RAPP-containing arrest peptides induce translational stalling by short circuiting the ribosomal peptidyltransferase activity. *Nat. Commun.* **15**, 2432 (2024).
51. Huter, P. et al. Structural Basis for Polyproline-Mediated Ribosome Stalling and Rescue by the Translation Elongation Factor EF-P. *Mol. Cell* **68**, 515–527.e6 (2017).
52. Turnbull, K. et al. The ABCF ATPase New1 resolves translation termination defects associated with specific $tRNA^{Arg}$ and $tRNA^{Lys}$ isoacceptors in the P site. *Nucleic Acids Res.* **52**, 12005–12020 (2024).
53. Goldman, D. H. et al. Mechanical force releases nascent chain–mediated ribosome arrest in vitro and in vivo. *Science* **348**, 457–460 (2015).
54. Nilsson, O. B. et al. Cotranslational Protein Folding inside the Ribosome Exit Tunnel. *Cell Rep.* **12**, 1533–1540 (2015).
55. Fujiwara, K., Katagi, Y., Ito, K. & Chiba, S. Proteome-wide Capture of Co-translational Protein Dynamics in *Bacillus subtilis* Using TnDR, a Transposable Protein-Dynamics Reporter. *Cell Rep.* **33**, 108250 (2020).
56. Singh, S. et al. Cryo-EM studies of the four *E. coli* paralogs establish ABCF proteins as master plumbers of the peptidyl-transferase center of the ribosome. *bioRxiv* **06**, 543498 (2023).
57. Chadani, Y., Niwa, T., Chiba, S., Taguchi, H. & Ito, K. Integrated in vivo and in vitro nascent chain profiling reveals widespread translational pausing. *Proc. Natl. Acad. Sci.* **113**, E829–E838 (2016).
58. Punjani, A., Rubinstein, J. L., Fleet, D. J. & Brubaker, M. A. cryoSPARC: algorithms for rapid unsupervised cryo-EM structure determination. *Nat. Methods* **14**, 290–296 (2017).
59. Zivanov, J. et al. New tools for automated high-resolution cryo-EM structure determination in RELION-3. *eLife* **7**, e42166 (2018).
60. Pettersen, E. F. et al. UCSF Chimera—A visualization system for exploratory research and analysis. *J. Comput. Chem.* **25**, 1605–1612 (2004).
61. Liebschner, D. et al. Macromolecular structure determination using X-rays, neutrons and electrons: recent developments in Phenix. *Acta Crystallogr. Sect. D.* **75**, 861–877 (2019).
62. Emsley, P., Lohkamp, B., Scott, W. G. & Cowtan, K. Features and development of Coot. *Acta Crystallogr. Sect. D: Biol. Crystallogr.* **66**, 486–501 (2010).
63. Jumper, J. et al. Highly accurate protein structure prediction with AlphaFold. *Nature* **596**, 583–589 (2021).
64. Williams, C. J. et al. MolProbity: More and better reference data for improved all-atom structure validation. *Protein Sci.* **27**, 293–315 (2018).
65. Meng, E. C. et al. UCSF ChimeraX: Tools for structure building and analysis. *Protein Sci.* **32**, e4792 (2023).
66. Case, D. A. et al. Amber 2024, University of California, San Francisco (2024).

Acknowledgements
We thank Takashi Kanamori for providing customized PURE*frex* v1.0. This work was supported by Platform Project for Supporting Drug Discovery and Life Science Research (Basis for Supporting Innovative Drug Discovery and Life Science Research (BINDS)) from AMED grant number JP25am121002, support no. 3272 (ON), Japan Society for the Promotion of Science (JSPS) KAKENHI (Grant Numbers 22H02553 (YI), 26K01958 (YI), 23H02410 (YC), and 26H00007 (ON)), MEXT Grant-in-Aid for Scientific Research, Grant Number JP20H05925 (HT), Japan Foundation for Applied Enzymology (YC), Takeda Science Foundation (YC), Yamada Science Foundation (YC), Inamori Foundation (YC), Noda Institute for Scientific Research (YC), Senri Life Science Foundation (YC), JST, PRESTO, Grant Number JPMJPR24OC (YC), and Core Research for Evolutional Science and Technology (CREST) of the Japan Science and Technology Agency (JST) (Grant Number JPMJCR20E2 (ON)).

Author contributions
Conceptualization: YC, YI Methodology: TF, YC, YI Investigation (cryo-EM): KI, YA, FKS, YI Investigation (mutational analysis): KY, YC Investigation (molecular dynamics): TI, TF Visualization: KI, TI, YC, YI Supervision: HT, ON, YC, YI Writing—original draft: YC, YI Writing—review & editing: KI, TI, TF, HT, ON, YC, YI.

Competing interests
The authors declare no competing interests.

Additional information
Supplementary information The online version contains supplementary material available at https://doi.org/10.1038/s41467-026-72863-1.

Correspondence and requests for materials should be addressed to Hideki Taguchi, Osamu Nureki, Yuhei Chadani or Yuzuru Itoh.

Peer review information *Nature Communications* thanks Sean Connell and the other, anonymous, reviewer(s) for their contribution to the peer review of this work. A peer review file is available.